SIMULATION OF THE INTERNAL CONDITIONS DURING THE HOT-PRESSING PROCESS

Balázs G. Zombori†
Research Scientist

Frederick A. Kamke†
Professor
Department of Wood Science and Forest Products
Virginia Polytechnic Institute and State University
Blacksburg, VA 24061-0503

and

Layne T. Watson
Professor
Departments of Computer Science and Mathematics
Virginia Polytechnic Institute and State University
Blacksburg, VA 24061-0106

(Received February 2002)

ABSTRACT

The development of a two-dimensional mathematical model to describe the internal conditions during the hot-compression of wood-based composite panels is discussed. Five primary variables were considered during the model development: air content, vapor content, bound water content, and temperature within the mat, and the extent of the cure of the adhesive system characterized by the cure index. Different heat and mass transfer processes were identified for the transport of the heat and of the moisture phases. The heat was transported by conduction and convection due to a temperature gradient, while the water phases were transported by bulk flow and diffusion due to total pressure and partial pressure gradients. The resulting differential-algebraic equation system was solved by the method of lines. The spatial derivatives of the conduction terms were discretized by central differences, while the spatial derivatives of the convection terms were discretized according to an upwind scheme. The resulting ordinary differential equations in the time variable were solved by a freely available differential-algebraic system solver (DDASSL). The mathematical model predicted temperature, moisture content, partial air and vapor pressures, total pressure, relative humidity, and extent of adhesive cure within the mat structure under a typical hot-compression process. A set of three-dimensional profiles describes the evolution of these variables with time, in the thickness and width dimensions of the mat. The model results allow a better understanding of the interacting mechanisms involved in a complex production process. The model also supports optimization of the hot-pressing parameters for improved quality of wood-based panel products, while reducing pressing time.

Keywords: Wood-based composites, heat and mass transfer, hot-pressing, process simulation, finite difference method.

INTRODUCTION

A composite panel attains its final characteristics during hot-pressing, as the loosely formed flake mat is compressed to its final thickness under elevated temperature and pressure. During the hot-pressing cycle, the internal conditions of the mat change rapidly. Heat is transported by conduction from the hot platens to the mat surface. The abrupt increase of temperature vaporizes the moisture content of the flakes at the surface and increases the vapor pressure. The pressure differential drives

† Member of SWST.

Wood and Fiber Science, 35(1), 2003, pp. 2–23

the hot vapor to the cooler center of the mat, where it may condense. Therefore, a vertical water vapor flow from the surface of the board towards the center can be observed at the beginning of the press cycle. As the rate of moisture evaporation at the surface declines, the surface temperature quickly reaches the platen temperature. However, it takes a considerable time to increase the centerline temperature of the mat to the local boiling point of water at the given internal pressure. As the center reaches this temperature, the water vaporization is accelerated, and the increased pressure in the center of the board will drive the vapor horizontally towards the exposed edges of the mat. The centerline temperature remains nearly constant until the moisture content drops considerably in the mat structure, due to the energy consumed by the vaporization process (latent heat). Consequently, the vertical flow accelerates the temperature rise in the center, while the horizontal flow retards it.

The rate of the vertical and horizontal mass transfer process is dominated by the flow of the water vapor through the porous structure of the mat. A structural model described in a related article (Zombori et al. 2001) is capable of predicting the dynamic structural changes within the mat during the press closure. Generally, the voids between the flakes are eliminated, and the porous structure of the flakes is also compressed during the press closing time. The substantial change in mat structure will affect the rate of the mass transfer through the changing physical mat properties. Therefore, it is crucial to link the mat structural properties to the mat transport and physical properties in the model.

The moisture distribution develops as a response to the temperature gradient. Consequently, the movement of moisture in the form of steam influences the temperature gradient during the press cycle; the heat and mass transfer are coupled. Evaporation and condensation of the moisture in the mat will consume or release latent energy, respectively, which contributes to temperature and gas pressure changes. The result of these interacting heat and mass transfer mechanisms is a three-dimensional variation in temperature, moisture content, and pressure within the mat structure. The viscoelastic properties of the flakes, such as the relaxation modulus, depend on the moisture content and temperature variation. The rate and extent of the cure of the thermosetting resin are also functions of the mat internal conditions. The production parameters substantially affect the internal environment of the mat and the final characteristics of the manufactured board. If the connection between production parameters and the final properties is established, the process operators can have a great influence on the ultimate properties of the board. Therefore, it is critical to describe the changes of moisture content and temperature within the flake mat in space and time. This article focuses on the development of a numerical simulation model to describe the heat and mass transfer phenomena within the mat structure during a conventional hot-pressing operation. The comparison of the model predicted and measured internal mat conditions among a wide range of pressing parameters, and the simulation and validation of the vertical density profile formation will be reported in subsequent articles.

BACKGROUND

Two complementary approaches have emerged to find relationships between production parameters and the properties of wood-based composite panels: testing and modeling. A number of investigators studied the hot-compression process based on empirical data collected on a small scale laboratory press (Kelley 1977; Strickler 1959; Maku et al. 1959; Kamke and Casey 1988a, b). Sophisticated experimental designs were constructed to statistically analyze the effect of platen temperature, initial moisture content, panel final density, and other variables on certain board properties. An inherent disadvantage of this approach is that, although general trends can be observed, the data are valid only for the range of testing conditions. In order to remedy

the drawbacks of the experimental approach, several numerical models were developed in the last three decades to better understand the transient effects during the hot-compression process of wood-based composites.

One of the earliest attempts to model temperature and moisture distribution in particleboard in two dimensions was that of Bowen (1970). He used measured temperature data and a finite difference model to predict the contribution of sensible (conduction) and latent (condensation/evaporation) heat on the heat transfer in the mat. Latent heat was calculated by deducting the calculated sensible heat from the experimental temperature data. Having evaporation and condensation rates, moisture distributions within the mat structure were calculated at various stages of the press cycle. Bowen concluded that, in addition to the conduction component, the heat of resin polymerization plays an important role. Radiation effects and heat of compaction were also proposed as contributing to the thermal history of the mat.

In an extensive review on the hot-pressing of plywood and particleboard, Bolton and Humphrey (1988) identified the primary physical processes and their interactions. Several related papers (Humphrey 1989; Bolton et al. 1989a, b, c) described the derivation and validation of the most comprehensive simulation model to date for heat and moisture transfer during the hot-pressing of particleboard. Conduction, convection, bulk flow, and water phase change were the heat and mass transfer mechanisms included in the model. The two-dimensional, time-dependent problem in a cylindrical coordinate system was solved by the finite difference method, assuming that steady-state theory adequately describes the behavior of the system during each time increment. Temperature, steam pressure, and equilibrium moisture content were predicted in the radial and vertical directions. The internal environment at the corner of the board was calculated by interpolating results obtained from inscribed and circumscribed cylinders of the rectangular shape of the board. The model neglected the effect of press closing time and resin cure on the internal environment of the mat. Instead, instantaneous press closing was assumed, and variables were predicted only for the remaining part of the press schedule. The vertical density gradient formation during mat consolidation was not considered, but rather they assumed a stepwise change of the density profile at certain stages of the compression process. Therefore, the transfer properties also changed stepwise in the model, causing some numerical difficulties.

Harless et al. (1987) were among the first who recognized the relationship between the vertical density profile formation and the internal temperature and pressure distribution in the board. A model was developed to simulate the effect of heat and moisture on development of the vertical density profile. They considered only conduction heat transfer and mass transfer by bulk flow. The compressibility of the flakes was assumed to be only a function of temperature. The simulated pressing process was terminated as the final thickness of the mat was reached, not accounting for the effect of the differential relaxation of the mat during the remaining part of the press schedule.

Kayihan and Johnson (1983) developed a one-dimensional model for the combined heat and mass transfer in particleboard. Conduction and convection heat transfer, and bulk-flow mass transfer were considered together with water phase equilibrium equations in the model. The edge effect, losing moisture and heat at the edge of the board, was taken into consideration by a "leakage" term.

Carvalho and Costa (1998) developed a three-dimensional model for the hot-pressing of medium density fiberboard (MDF). The equations were based on the Stanish (1986) drying model, but the physical properties were assessed for fiberboard instead of solid wood. Although the temperature and moisture effects on the physical properties were included, the effect of press closing on the structure, and consequently on the physical properties of the mat, was neglected. The predicted results closely followed general temperature and

moisture content trends during a typical hot-pressing process, as was demonstrated by comparing the results to other model predictions.

Dai et al. (2000) presented a comprehensive mat consolidation model based on general physics and mechanics concepts. The model connected the mat formation, heat and mass transfer, and consolidation stress-strain behavior of the mat in order to predict the resulting density profile of the final panel. Good agreement was found between model predicted and experimental vertical density profiles.

A numerical continuous hot-press model was introduced by Humphrey and Thoemen (2000). The heat and mass transfer properties (conductivity, permeability) and the rheological characteristics of the mat were determined experimentally. The results of a simulation run provided good qualitative agreement with the expected behavior of the temperature and gas pressure inside the mat.

It is apparent that previous models had inherent limitations; either they were one-dimensional, or gross simplifications were made about the transfer mechanisms. In this work, a general approach was followed during the model development, which allowed a comprehensive description of the heat and mass transfer phenomena during hot-pressing. All conceivable simultaneous heat and mass transfer mechanisms were considered, together with phase balancing sorption isotherms. By numerically solving the governing equations, the prediction of the evolution of moisture and temperature profiles in the vertical midplane of the board became attainable. The changing internal environment of the mat allows the assessment of the viscoelastic (time-temperature-, and moisture-dependent) response of the flakes and the simulation of the vertical density profile formation, which will be discussed in a separate paper.

MODEL DEVELOPMENT

Assumptions

The one-dimensional drying model published by Stanish et al. (1986) formed the basis for further model development. The model was extended to two spatial dimensions, and the transport properties were changed to incorporate the differences between solid wood and oriented strandboard mat properties. Several simplifying assumptions were adopted to solve the problem imposed by the coupled heat and moisture transfer mechanisms during hot-pressing:

– Solid and gaseous phases are considered, and these two phases are always in local thermodynamic equilibrium.

– Heat and mass transfer between the two phases are instantaneous; therefore, any resistance between the solid and gas phase is neglected.

– The gas phase is composed of an air-water vapor mixture, and the components follow the Ideal Gas Law.

– Air is treated as a single component gas.

– Water can be present as bound water in the cell wall or water vapor in the voids; the free water component is ignored due to the low initial mat moisture content typical for wood composite manufacture.

– The bound water in the cell walls is always in local equilibrium with the water vapor in the voids.

– The heat supply for the process comes from the hot-press platens and from the heat of reaction of the resin.

– Water produced during the condensation reaction of the resin is neglected.

– The physical and transport properties are functions of temperature, moisture content, density, porosity, and steam pressure; therefore they may vary with respect to space and time.

– The press schedule includes the press closing period during which the porosity and density of the mat changes continuously, resulting in changes of the physical and transport properties of the mat.

– Conditions at the four boundaries are independent of each other and can vary with time.

– The mechanisms for heat and mass transfer are:

a.) Heat is transported by conduction due to temperature differential and by bulk flow of the air and water components.

b.) The two gas phases (air and vapor) are transferred by bulk flow and diffusion, and follow Darcy's Law and Fick's Law, respectively; the driving force of the bulk flow is the total pressure differential, while the driving force of diffusion process is the partial pressure differential.

c.) The migration of the bound water occurs by molecular diffusion due to a gradient in chemical potential of the bound water molecules.

d.) Phase change of water from the adsorbed to the vapor phase is implicitly included in the energy equation as latent heat of vaporization.

Governing equations

The description of various transport phenomena involved in a conventional hot-pressing process involves the solution of mass and energy conservation equations. The model equations contain five dependent variables and five governing equations. The five dependent variables are the air density (ρ_a), water vapor density (ρ_v), bound water density (ρ_b), temperature (T), and the cure index of the adhesive (F). The mass density terms are based on the volume of the mat. The five variables are functions of three independent variables: thickness (z), width (y), and time (t). The five governing equations include two mass balance equations (one for air, and one for the moisture phase), one energy balance equation, one phase equilibrium equation, and one adhesive cure kinetics equation. (The description of variables, subscripts, and superscripts in the equations is given in the nomenclature.)

The constitutive equations are the mass conservation equation for air

$$\frac{\partial}{\partial t}(\rho_a) = -\nabla\cdot n_a, \tag{1}$$

the mass conservation equation for the water phase

$$\frac{\partial}{\partial t}(\rho_v + \rho_b) = -\nabla\cdot(n_v + n_b), \tag{2}$$

the energy balance equation

$$\frac{\partial}{\partial t}(\rho_a\cdot h_a + \rho_v\cdot h_v + \rho_b\cdot h_b + C\cdot T) = -\nabla\cdot(n_a\cdot h_a + n_v\cdot h_v + n_b\cdot h_b + q) + G, \tag{3}$$

the phase equilibrium relation, which is an inverted form of the Hailwood-Horrobin two-hydrate sorption model (Hailwood and Horrobin 1946; Simpson 1971, 1973, 1980),

$$\rho_v = \rho_v^{\text{sat}}\left[Z_1 + \left(Z_1^2 + \frac{1}{K_1K_2^2}\right)^2\right], \tag{4}$$

where

$$K_1 = -45.70 + 0.3216T - 5.012\cdot10^{-4}T^2,$$

$$K_2 = -0.1722 + 4.732\cdot10^{-3}T - 5.553\cdot10^{-6}T^2,$$

$$W = 1417\cdot10^3 - 9.430T + 1.853\cdot10^{-2}T^2,$$

$$Z_1 = \frac{1 - Z_2}{2K_2} - \frac{1 + Z_2}{2K_1K_2}, \qquad Z_2 = \frac{18}{W\frac{\rho_b}{\rho_d}},$$

and the cure kinetics equation of the adhesive system (Scott 1989; Kiran and Iyer 1994)

$$\frac{\partial F}{\partial t} = Ae^{-(E/RT)}(1 - F)^n. \tag{5}$$

This set of coupled differential-algebraic equations forms the basis of the hot-pressing model. The numerical solution of the system provides the air content, vapor content, bound water content, temperature, and cure index as a function of time in two spatial dimensions.

Transport mechanisms

Heat transfer.—Heat conduction is described by Fourier's First Law

$$q = -k_m \frac{\partial T}{\partial x}. \tag{6}$$

The rate of the conduction heat transfer for a given temperature differential is determined by the thermal conductivity of the mat (k_m), which varies with the mat structure (flake density, flake orientation, void fraction) and with the internal environment.

Bulk flow has an important role to transport the energy content of the gas phases, most importantly the water vapor phase within the mat structure vertically and horizontally. The magnitude of the bulk flow contribution depends on the amount of water available and the void fraction. The voids in the mat create a pathway for bulk flow. The bulk flow terms in the energy equation are the product of the mass flux and the enthalpy of each phase

$$c = n_p h_p. \tag{7}$$

n_p designates flux terms for air, vapor, and bound water flow, and h_p is the enthalpy, where the subscript p is a (air), b (bound water), or v (vapor).

Heat is also generated by the exothermic polymerization reaction of the resin, which depends on the rate of the reaction

$$G = h_g \rho_g \frac{\partial F}{\partial t}. \tag{8}$$

Mass transfer.—Only two water phases are assumed to be present, water vapor filling the cell lumens and the space between the flakes, and bound water hydrogen-bonded to the cell-wall material. Because of the low initial moisture content of the mat (maximum 12%), it is unlikely that free (liquid) water would be present in the voids at the beginning of the pressing process. The assumption of local thermodynamic equilibrium will not allow the presence of liquid water except in rare cases.

The two main mass phases in the mat are the vapor-air gas mixture in the cell lumens and in the space between the flakes, and the bound water in the cell wall. The transport mechanisms for each of the phases are derived considering the most general case feasible. The gaseous phase (vapor and air) is transported by two mechanisms within the mat and to the surrounding environment: by bulk flow due to total pressure differential and diffusion due to partial pressure differential. Darcy's Law was used to describe the bulk flow, and the diffusion component was assumed to follow Fick's Law. Therefore, the transport mechanism for the vapor phase is given by the combination of Darcy's Law and Fick's Law as shown by the general form in one dimension

$$n_v = -K_m \frac{\partial}{\partial x}(P) - D_m \frac{\partial}{\partial x}\left(\frac{p_v}{P}\right), \tag{9}$$

where the total pressure P is the sum of the partial pressures p_p, the mat superficial permeability is given by

$$K_m = \frac{\rho_v K_g}{\zeta_{vm} \eta_g}, \tag{10}$$

and the mat diffusivity is given by

$$D_m = \frac{M_v}{\zeta_{vm}}\left(\frac{\rho_a}{M_a} + \frac{\rho_v}{M_v}\right) D_{\text{eff}}. \tag{11}$$

Analogous mechanisms (bulk flow and diffusion) transport the air in the mat structure; therefore the equations are the same, but the subscript v is interchanged with the subscript a. The rate of the bulk flow and diffusion of vapor or air through the porous structure of the mat is determined by the mat superficial permeability (K_m) and the mat diffusivity (D_m), which in turn depend on the specific gas permeability (K_g) and effective diffusivity (D_{eff}), respectively. The specific gas permeability (K_g) and the effective diffusivity (D_{eff}) are functions of the mat structure, especially the amount of void present in the structure. As a result, the magnitude of these properties varies widely among different types of boards and during the press closure.

The bound water in the cell wall is trans-

ported by diffusion as described by Schajer et al. (1984) and follows Fick's Law with chemical potential as the driving force:

$$n_b = D_b(1 - \zeta_{vm})\frac{\partial \mu_b}{\partial x}. \quad (12)$$

Since thermodynamic equilibrium is assumed at every point of the mat, the chemical potential of the bound water (μ_b) by definition is equal to the chemical potential of water vapor (μ_v).

Phase equilibrium

The most widely used model to describe phase equilibrium in a wood and water system is the two-hydrate form of the Hailwood-Horrobin equation (Hailwood and Horrobin 1946) with parameters fitted by Simpson (1973). However, it was demonstrated that the model is not valid above 160°C. Data on the high temperature sorption characteristics of wood are limited (Lenth and Kamke 2001; Kauman 1956; Simpson and Rosen 1981). Consequently, an inverted form of the Hailwood-Horrobin two-hydrate model was used to keep the balance between the vapor and the bound water phases below 160°C (Eq. (4)), and cubic splines interpolants to the data of Kauman (1956) were used to describe the sorption relationship at high temperature.

Material properties

Transport properties.—An important aspect of the behavior of wood-based composites is that the transport properties of the material are direction-dependent. Three principal axes (in-plane forming and crossforming directions, and out-of-plane thickness direction) can be identified in an oriented strandboard mat, giving an orthotropic symmetry to the material. A further simplification into a two-dimensional model requires transport properties to be determined only in the out-of-plane (thickness) and in-plane (width) directions of the mat. A considerable improvement on previous models is the inclusion of the press closing in the simulated press schedule since all the mat transport properties are affected by the changing mat structure during this period of the hot-compression. Local variation of the transport properties with changing void volume in the mat structure was not assessed; instead the variation of the void fractions in the whole mat was linked to the varying transport properties during the press closure. Additionally, the transport properties are a function of the varying temperature and moisture content in the mat structure. The effect of flake orientation on the thermal conductivity of the mat was also included. The transport properties of the mat were estimated using data from the literature for solid wood or particleboard. The experimental determination of these transport properties can considerably improve the model predictions.

The thermal conductivity of the mat was based on the thermal conductivity of solid wood, the thermal conductivity of air, and the structure of the mat. The specific gravity and moisture content dependence of the solid wood thermal conductivity in the transverse (radial and tangential) direction was given by Siau (1995) as

$$k_T = SG(k_{cw} + k_w \cdot M) + k_a v, \quad (13)$$

where

SG = specific gravity of wood,
k_{cw} = conductivity of cell-wall substance (0.217 J/m/s/K),
k_w = conductivity of water (0.4 J/m/s/K),
k_a = conductivity of air (0.024 J/m/s/K),
M = moisture content of wood (fraction),
v = porosity of wood.

Substituting model variables yields

$$k_T = \frac{\rho_f}{1000}\left(k_{cw} + k_w\frac{\rho_v + \rho_b}{\rho_d}\right) + k_a\zeta_{lf}. \quad (14)$$

The flake density (ρ_f) together with the thermal conductivity increased in the model as the mat was compressed and the flakes were densified. The longitudinal thermal conductivity of solid wood was assumed to be 2.5 times higher than the transverse conductivity (Siau 1984). It was assumed that the conductivity of

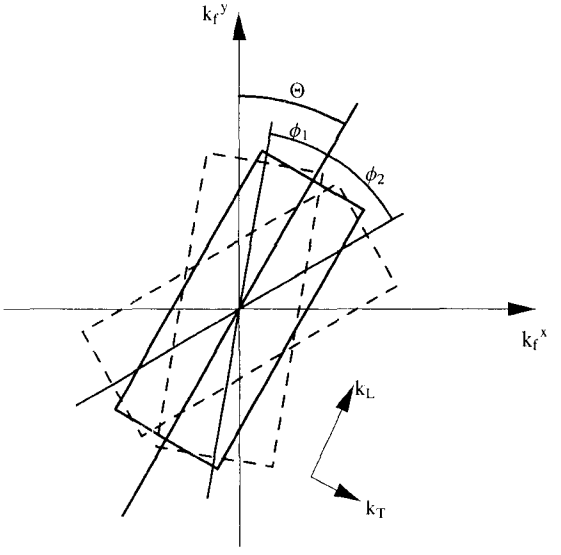

FIG. 1. The effect of the orientation angle (Θ), and degree of alignments (ϕ_1, ϕ_2) on the thermal conductivity of the flakes at the in-plane direction of the mat.

the flakes in the two main anatomical directions can be calculated by the corresponding thermal conductivity of solid wood. However, the flakes are intentionally rotated to a certain orientation angle (Θ) during the deposition process. Therefore, the magnitude of the thermal conductivity will be between the longitudinal and transverse values in the two perpendicular in-plane board directions. The deposition process is not exact. The orientation angle will fill a range of values, which can be quantified with the degree of alignments (ϕ_1, ϕ_2). The orientation angle (Θ) and degree of alignments (ϕ_1, ϕ_2) are depicted in Fig. 1. The degree of alignment is zero for perfect alignment, when the flakes are positioned at the orientation angle (Θ), and increases as the rotation of the flakes deviates from the intended orientation. The dependence of thermal conductivity on the orientation angle and the degree of alignment in the in-plane (y) direction is described by the function

$$k_f^y = \frac{1}{2}\left|\cos(\Theta + \phi_1)k_L - \sin(\Theta + \phi_1)k_T + \cos(\Theta + \phi_2)k_L - \sin(\Theta + \phi_2)k_T\right|. \quad (15)$$

The thermal conductivity of the flakes in the thickness direction (z) is independent of rotation angle and equal to the conductivity of solid wood in the transverse (radial and tangential) direction (Eq. (14)).

The loosely formed mat structure consists of strands and space among the strands due to the inherent randomness of the mat formation. The magnitude of the space is described by the space fraction of the mat (ζ_{sm}) in the previously published mat formation model (Zombori et al. 2001). The air-filled space acts as a thermal insulator during the press closure. As the pressing proceeds, the space is eliminated from the structure, and when the mat reaches the target thickness, practically no space remains in the mat. Therefore, after reaching the target thickness of the panel, the thermal conductivity of the mat will be that of the compressed strands. It was assumed that the air-filled space and the strands form a parallel system of thermal resistance in the in-plane, and a serial system of thermal resistance in the out-of-plane directions of the mat. Therefore, the thermal conductivity of the mat in two perpendicular directions is given by

$$k_m^y = k_a\zeta_{sm} + k_f^y(1 - \zeta_{sm}), \quad (16)$$

$$k_m^z = \frac{k_a k_T}{k_a(1 - \zeta_{sm}) + k_T\zeta_{sm}}. \quad (17)$$

Permeability is an important property that determines the rate of gas flow in the mat structure during hot-pressing. In particulate composites, such as OSB and particleboard, permeability is closely related to the mat density or porosity. In spite of its known effect on the internal environment of the mat, there has not been much research related to permeability of wood composites (Smith 1982; Hata 1993; Hata et al. 1993; Bolton and Humphrey 1994; D'Onofrio 1994). Specific permeability data of particleboard in the thickness (out-of-plane) direction as a function of board density were presented by Humphrey (1989). An exponential curve was fit to the permeability data by Carvalho and Costa (1998), and this function was used to describe the structure

dependence of the specific permeability of the mat in the model in the out-of-plane direction,

$$K_g^z = 1.74 \cdot 10^{-12} \exp(-8.06 \cdot 10^{-3} \rho_{mat}). \quad (18)$$

Humphrey (1989) also established a ratio of 59:1 for the permeability parallel and normal to the board plane. The parallel (in-plane) data were based on permeability measurements on extruded particleboards. In the absence of a more reliable relationship, this ratio was considered in the whole density range.

Diffusion occurs due to a partial pressure differential in the mat. The interdiffusion coefficient of an air-vapor mixture (binary gas diffusion coefficient) is calculated by the semi-empirical relationship (Stanish et al. 1986; Incropera and Dewitt 1996)

$$D_{AB} = 2.20 \cdot 10^{-5} \left(\frac{101{,}325}{P}\right)\left(\frac{T}{273.15}\right)^{1.75} \quad (19)$$

To take into account the porous structure of the mat, this value is reduced by the square of the void fraction (Bejan 1986). Therefore, the random pore gas diffusivity for porous solids, such as a flake mat, is expressed as

$$D_{rp} = \zeta_{vm}^2 D_{AB}. \quad (20)$$

In the mat, the void structure presents a tortuous path for gas flow, which is taken into consideration by an empirical attenuation factor α. The attenuation factor was set at a value of 0.5 (Stanish et al. 1986) in both the vertical and horizontal directions, assuming that the pathway is similar for diffusion horizontally and vertically in the mat structure,

$$D_{eff} = \alpha D_{rp}. \quad (21)$$

Although the directional dependence of the diffusion might improve the model predictions, it was not included in the model. Generally, diffusion compared to bulk flow has a small role in the gas phase transport in the mat, and its directional dependence was disregarded.

Bound water diffusivity in solid wood was assumed to be constant at $3 \cdot 10^{-13}$ kg·s/m^3, following the results of Stanish et al. (1986), and given the expected temperature and moisture content range during hot-pressing.

Physical properties.—The specific heat of wood and its associated moisture content are an integral part of the energy balance equation. The density, temperature, and moisture-dependence of the specific heat was given by Skaar (1972) as

$$C = \frac{\rho_d}{1000} \times \frac{\left[0.268 + 0.0011(T - 273.15) + \frac{\rho_b + \rho_v}{\rho_d}\right]}{0.293}. \quad (22)$$

The viscosity of the air-vapor mixture is necessary to calculate the superficial gas permeability of the mat. The dependence of viscosity on temperature and partial pressure is given as the linear combination of the component viscosities weighted by the mole fractions in the mixture, resulting in the equation (Stanish et al. 1986)

$$\eta_g = [(6.36 \cdot 10^{-6} + 4.06 \cdot 10^{-8} T) p_a + (-1.57 \cdot 10^{-6} + 3.80 \cdot 10^{-8} T) p_v]/P. \quad (23)$$

The saturated vapor density is included in the inverted form of the Hailwood-Horrobin model (Eq. (4)), which was used to calculate the relative humidity within the mat. The temperature-dependence of the saturated vapor density is described by an exponential curve fitted to experimental saturated vapor pressure data (Stanish et al. 1986)

$$\rho_v^{sat} = \zeta_{vm} \exp(-46.490 + 0.26179T - 5.0104 \cdot 10^{-4} T^2 + 3.4712 \cdot 10^{-7} T^3). \quad (24)$$

Cure properties of the adhesive.—The adhesive cure kinetics is described by an Arrhenius-type equation (Eq. (5)). The equation assumes a single-step reaction, which is an oversimplification, but it fits experimental data for the cure for specific thermoset adhesive formulations

very well. This equation establishes the relationship between temperature and the extent of the polymerization of the thermosetting resin. The parameters in the equation have to be determined empirically for each adhesive system. The activation energy of the reaction (E), the reaction constant (A), and the order of the reaction (n) were determined for a commercial phenol-formaldehyde face adhesive by Ahmad (2000) using the same procedure and equipment described by Sernek et al. (2000), resulting in A = 0.25 l/s, E = 12423 J/mol, n = 0.587.

Thermodynamic relationships

For the air, vapor, bound water, and adhesive phases within the mat an enthalpy function was defined (Stanish et al. 1986). The enthalpy of air was determined to be only a function of temperature

$$h_a = C_a(T - 273.15), \tag{25}$$

where

C_a = air heat capacity (1000 J/kg/K).

The enthalpy of water vapor was calculated as the sum of the enthalpy of the liquid phase of water, heat of vaporization, and enthalpy of the gas phase of water as

$$h_v = C_{lw}(T_{dp} - 273.15) + \lambda_{dp} + C_{gw}(T - T_{dp}), \tag{26}$$

where

C_{lw} = liquid water heat capacity (4180 J/kg/K),
C_{gw} = vapor heat capacity (1950 J/kg/K).

Heat of vaporization data from steam tables was fitted to a polynomial as a function of temperature (Stanish et al. 1986)

$$\lambda = 2.792 \cdot 10^6 - 160T - 3.43T^2. \tag{27}$$

Dewpoint temperature as a function of partial vapor pressure was described by:

$$T_{dp} = 230.9 + 2.10 \cdot 10^{-4} p_v - 0.639\sqrt{p_v} + 6.95\sqrt{p_v^3}. \tag{28}$$

After substituting Eq. (28) into Eq. (27) and Eq. (27) into Eq. (26), the enthalpy of water vapor is given by

$$h_v = 1.65 \cdot 10^6 + 1950T - 2070T_{dp} - 3.43T_{dp}^2. \tag{29}$$

The differential enthalpy of bound water is equal to free water enthalpy less the differential heat of sorption. The differential heat of sorption decreases quadratically with increasing bound water content. At zero bound water content ($\rho_b = 0$) it was considered to be 40% of the heat of free water vaporization (Stanish et al. 1986)

$$h_b = C_{lw}(T - 273.15) - 0.4\lambda\left(1 - \frac{\rho_b}{\rho_b^{fsp}}\right)^2, \tag{30}$$

where

C_{lw} = liquid water heat capacity (4180 J/kg/K),
ρ_b^{fsp} = bound water density at fiber saturation.

According to the previous relationship, at full saturation ($\rho_b = \rho_b^{fsp}$), the differential enthalpy of bound water reaches a maximum, and decreases as the bound water is depleted. The heat capacities (C) were considered to be constant in the previous relationships, but in future models the temperature dependence of the heat capacities can be included.

The heat of reaction (h_g) of the adhesive system was taken from the literature (Myers et al. 1991; Holopainen et al. 1997). Differential scanning calorimetry (DSC) data describe the energy generation of the exothermic reaction during the polymerization of the thermosetting resin. These data show distinct peaks as the reaction enters different stages. Therefore a total heat of reaction value was calculated as the area under the DSC curve, and had the value of $3 \cdot 10^5$ J/kg in the model.

Initial and boundary conditions

Solution of the mass conservation and energy balance equations (Eqs. (1)–(5)) requires one initial and four boundary conditions. From the

initial moisture content of the mat and the temperature of the ambient air, the initial conditions are calculated by satisfying the local thermodynamic and phase equilibrium constraints,

$$T(y, z, 0) = T^0, \quad (31)$$

$$\rho_a(y, z, 0) = \rho_a^0, \quad (32)$$

$$\rho_v(y, z, 0) = \rho_v^0, \quad (33)$$

$$\rho_b(y, z, 0) = \rho_b^0. \quad (34)$$

The boundary conditions are obtained from the heat and moisture transfer phenomena between the surfaces and edges of the board and the external environment. The boundary conditions for the four surfaces are independent of each other and they can vary with time in the model. Although this assumption increases computational time, it also allows the simulation of nonsymmetric boundary conditions, and the simulation of industrial press closure, where the bottom and top surfaces will experience different time-temperature histories due to the press daylight. The following equations specify the boundary heat and mass fluxes at the top and bottom surfaces and left and right edges of the mat. The heat transfer at the boundaries was assumed to follow Newton's Law of cooling

$$q^j = -\mathcal{H}^j(T^{j,\infty} - T^B), \quad (35)$$

where j refers to the top, bottom, left, or right boundary.

The mass transfer of the gas phase (air and water) is a combination of bulk flow and diffusion, due to total pressure and partial pressure difference between the surface of the board and the ambient environment:

$$n_a^j = -\rho_a \frac{\mathcal{K}^j}{\eta_g}(P^{j,\infty} - P^B) - M_a\left(\frac{\rho_a}{M_a} + \frac{\rho_v}{M_v}\right)\mathcal{D}^j(p_a^{j,\infty} - p_a^B), \quad (36)$$

$$n_v^j = -\rho_v \frac{\mathcal{K}^j}{\eta_g}(P^{j,\infty} - P^B) - M_v\left(\frac{\rho_v}{M_v} + \frac{\rho_a}{M_a}\right)\mathcal{D}^j(p_v^{j,\infty} - p_v^B). \quad (37)$$

The bound water flux is zero at the boundary:

$$n_b^j = 0. \quad (38)$$

Setting the bound water flux to zero at the boundary implies that the water in the bound phase can not leave the mat structure; it has to be vaporized before it can escape to the environment. The boundary temperatures ($T^{j,\infty}$) are that of the hot plate temperature on the surface (top and bottom) boundaries and the ambient air temperature on the edge (left and right) boundaries of the mat. Variation of surface temperature of the hot platen, due to nonuniform heating, and variation of temperature at the edges of the mat, due to the effect of the escaping hot vapor, might be present during the hot-compression. This may be simulated in the model, but these effects are assumed to be negligible. The total pressure ($P^{j,\infty}$) was considered to be constant at 101,325 *Pa*.

By adjusting the external heat and mass transfer coefficients ($\mathcal{H}^j$, $\mathcal{K}^j$, $\mathcal{D}^j$), the rate of temperature change at the boundaries and the amount of water leaving the mat can be controlled. The heat transfer is fast from the hot platens to the surface of the mat, which is indicated by high external heat transfer coefficients. However, only a small amount of water can leave the mat towards the metal plates. Therefore, low external mass transfer coefficients are assumed at the platen. The contrary is true for the edge boundaries, where the heat transfer is slower, and the mass transfer is far faster, indicating that the majority of the water vapor leaves the mat through the edges.

NUMERICAL SOLUTION

The method of lines with finite differences in space was chosen for solution of the equation system (Eqs. (1)–(5)), because it is especially effective and convenient when the model has regular geometry with simple boundary conditions. The partial differential equations (PDEs) were discretized in the spatial variables using a control volume formulation as shown in Fig. 2. Central differences were used for the discretization of the conduction terms and an upwind scheme for the bulk flow terms

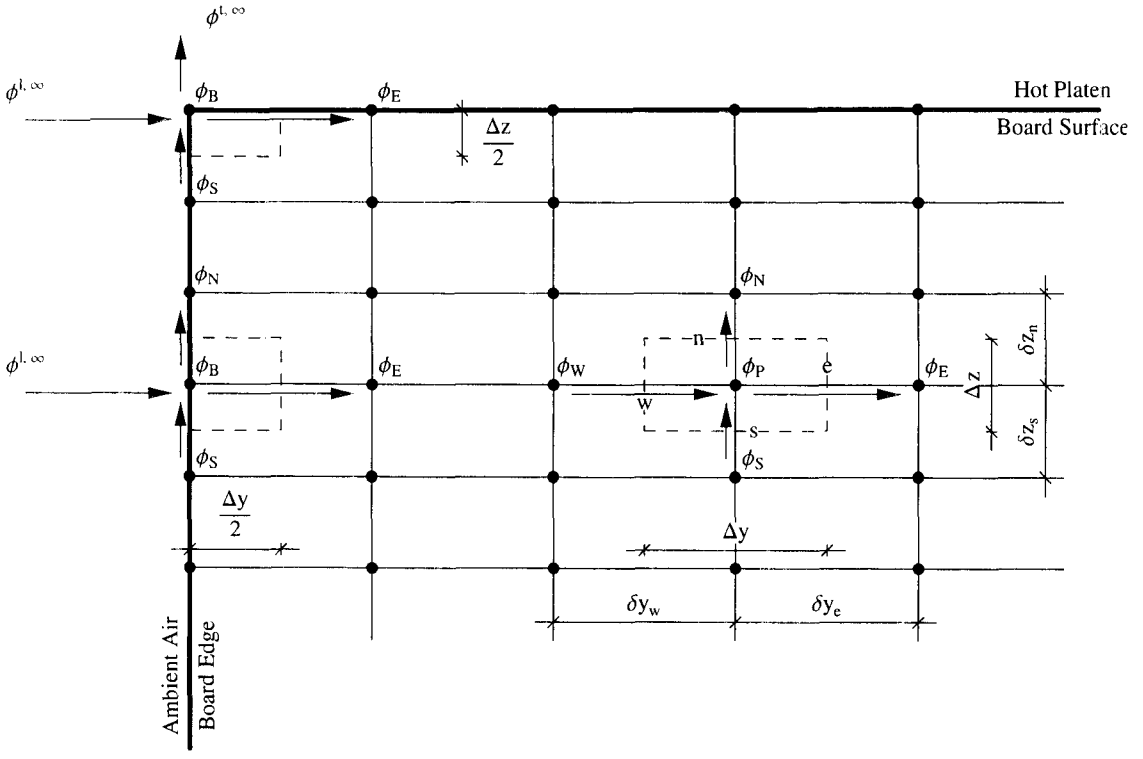

FIG. 2. The finite difference mesh superimposed on the vertical midplane of the board (ϕ designates any dependent variable at the mesh point).

as described in detail by Patankar (1980). The resulting ordinary differential equations (ODEs), the algebraic sorption equation, and the adhesive cure kinetics equation were solved by the algebraic-differential time integrator DDASSL developed by Petzold and Ascher (1998). DDASSL is a specialized initial value problem solver that can handle algebraic equations in the system. The solver accepts the equations in implicit form. Another advantage of DDASSL is that the internal time steps and ODE method order are adjusted automatically, depending on the convergence and stability criteria of the problem. In the case of fast convergence, the internal time steps are increased, essentially reducing the computational time. The solver uses backward difference formulas, and the Jacobian matrix is approximated internally. The solution requires the calculation of the right-hand-side of the equations with a user-supplied subroutine. The main program calls the solver with the specified output time when values of the dependent variables are required. The vertical midplane of the board was discretized to 361 mesh points, 19 in each direction in the following case study. Although the problem is two-dimensional, nonlinear, and the number of equations is quite high, a solution was typically reached within an hour on a UNIX workstation (DEC Alpha).

RESULTS AND DISCUSSION

The previously described model can predict the evolution of temperature, moisture content, total pressure, partial air and vapor pressures, relative humidity, and extent of cure of the adhesive with time in the vertical midplane of the mat. Several simulations were completed under hypothetical pressing conditions to test the robustness of the model. It performed well

TABLE 1. *Hot compression parameters used in the simulation.*

Dry strand density	ρ_d	466	(kg/m^3)
Initial temperature	T_0	25	(°C)
Initial moisture content*	$M.C._0$	5	(%)
Permeability of the mat	K_g	$1.74 \cdot 10^{-12}$	(m^2)
Permeability ratio (K_g^z/K_g^y)	*KRatio*	59	
Diffusion attenuation factor	α	0.5	
Bound water diffusivity	D_b	$3 \cdot 10^{-13}$	(kg s/m^3)
Cell wall thermal conductivity	k_{cw}	0.217	(J/m/s/K)
Moisture thermal conductivity	k_w	0.4	(J/m/s/K)
Air thermal conductivity	k_a	0.024	(J/m/s/K)
Surface temperature	$T^{t,x}$, $T^{b,x}$	200	(°C)
Surface relative humidity	$RH^{t,x}$, $RH^{b,x}$	35	(%)
Surface total pressure	$p^{t,x}$, $p^{b,x}$	1	(bar)
Surface heat trans. coeff.	$\mathcal{H}^t$, $\mathcal{H}^b$	75	(J/m^2/s/K)
Surface bulk flow coeff.	$\mathcal{K}^t$, $\mathcal{K}^b$	$4 \cdot 10^{-13}$	(m)
Surface diffusion coeff.	$\mathcal{D}^t$, $\mathcal{D}^b$	$0.5 \cdot 10^{-6}$	(m/s)
Edge temperature	$T^{l,x}$, $T^{r,x}$	100	(°C)
Edge relative humidity	$RH^{l,x}$, $RH^{r,x}$	35	(%)
Edge total pressure	$p^{l,x}$, $p^{r,x}$	1	(bar)
Edge heat trans. coeff.	$\mathcal{H}^l$, $\mathcal{H}^r$	10	(J/m^2/s/K)
Edge bulk flow coeff.	$\mathcal{K}^l$, $\mathcal{K}^r$	$1 \cdot 10^{-6}$	(m)
Edge diffusion coeff.	$\mathcal{D}^l$, $\mathcal{D}^r$	1.5	(m/s)
Board width	L_y	609.6	(mm)
Board final thickness	L_z	19.05	(mm)
Press closing time	*Pct*	60	(s)
Press opening time	*Pot*	480	(s)
Total press time	*Ptt*	540	(s)
# of mesh points @ Y direction	*NmpY*	19	
# of mesh points @ Z direction	*NmpZ*	19	
Reaction constant	*A*	0.25	(l/s)
Activation energy	*E*	12423.0	(J/mol)
Order of the reaction	*n*	0.587	
Resin content**	ρ_g	24.4	(kg/m^3)
Resin average enthalpy	h_g	$3 \cdot 10^5$	(J/kg)

* includes water content of the resin.
** resin solid/compressed mat volume.

over a wide range of input parameters. The basic capabilities of the model are demonstrated on a single-layer strandboard hot-compression simulation for one type of mat and press schedule specification. A following paper will compare the model predictions with experimental data among a wide range of panel densities and pressing schedules. The structure of the mat was recreated by using the mat formation model of Zombori et al. 2001. The simulated mat was positioned in the "virtual hot-press" to further analyze the temperature, moisture, and internal gas pressure distribution in the vertical midplane of the panel. For the simulation run, the platen temperature, the temperature at the edge of the board, the relative humidity of the surrounding air, the initial moisture content and temperature of the board, and the press schedule were specified. These parameters, together with other simulation input parameters, are given in Table 1.

The time-dependent changes of the thermodynamic variables (temperature, moisture content, total pressure, relative humidity) and adhesive kinetics (cure index) can not be considered in isolation, because of their interaction. Several three-dimensional profiles of the basic variables were created at certain stages

of the hot-compression simulation to characterize the profound changes taking place in the internal environment of the mat. These profiles are largely qualitative, but provide a good graphical presentation of the time-dependent variations in the spatial conditions. The plots were generated by *Mathematica* (Wolfram 1992), which has been adapted for easy input of the data files. The evolution of temperature and moisture content in the vertical midplane of the panel is depicted in Fig. 3. Figure 4 gives the variation of total pressure and relative humidity at certain stages of the pressing schedule. Additionally, the two components of the total pressure, the air and vapor partial pressures, are shown in Fig. 5. Figure 6 summarizes the cure index data.

At the commencement of the hot-compression (0 s), the profiles show the defined initial and boundary conditions. The temperature of the mat is a uniform 25°C, and the high 200°C platen temperature at the surface and somewhat lower 100°C ambient temperature at the edge boundary of the board also can be observed. The moisture content is a uniform 5% within the mat structure, and very low (~0%) at the boundaries because of the specified low relative humidity and high temperature of the ambient environment (Fig. 3). The total pressure inside of the mat is in balance with the atmospheric pressure at the beginning of the compression process. The relative humidity is approximately 25% within the mat structure and approximately 2% at the boundaries (Fig. 4). Note that the main component of the gas phase in the mat initially is air. The vapor content is very low, indicated by the high air and low vapor partial pressures in the vertical midplane of the mat (Fig. 5). The adhesive reaction is not initiated, the cure index is 0 everywhere in the cross section of the mat (Fig. 6).

During the press closing period, the temperature increases sharply at the top and bottom surface of the board. It reaches a value close to the hot platen temperature soon after the press closing time (60 s). However, the center temperature is still low, forming a large temperature gradient in the vertical direction. The temperature gradient initiates conduction heat transport vertically from the hot platens to the cooler center. At this stage of the press schedule, the horizontal temperature differential is insignificant, resulting in only convection heat transfer in the horizontal direction. Notice the effect of the environment surrounding the edge of the board on the temperature distribution. The lower ambient temperature at the edge retards the temperature increase, essentially creating a lower edge than center temperature within the board (Fig. 3). Closest to the hot platens the temperature increases high enough that the activation energy of the polymerization reaction is reached and the adhesive cure begins to accelerate (Fig. 6). It is apparent in Fig. 5 that the growing temperature close to the hot platens will vaporize the moisture of the strands and will increase the partial vapor pressure considerably. The air component of the gas phase is forced out from the board as indicated by the sudden decrease in partial air pressure at the face location of the mat. The net effect is that the total pressure increases above the atmospheric pressure close to the hot platens (Fig. 4). The total pressure differential drives the vapor normal to the surface of the board. Except for a small fraction, the hot vapor can not escape towards the metal caul plates, but rather migrates vigorously by bulk flow and diffusion towards the center due to the total and partial vapor pressure gradient in the vertical direction (Fig. 4, Fig. 5). The movement of the water vapor front towards the center of the board can be traced on the relative humidity profile. The relative humidity gradually increases towards the center, and can reach high values (~60%) at certain locations (Fig. 4). An additional consequence of the quickly moving hot vapor is that the bulk flow plays a more significant role in the vertical heat transfer at this stage of the press schedule. The majority of the moisture is transported in the vapor phase. Nonetheless, a small (almost negligible) part of the vertical moisture movement is due to bound water diffusion in the cell wall of the strands, where the driving force is also the vertical tempera-

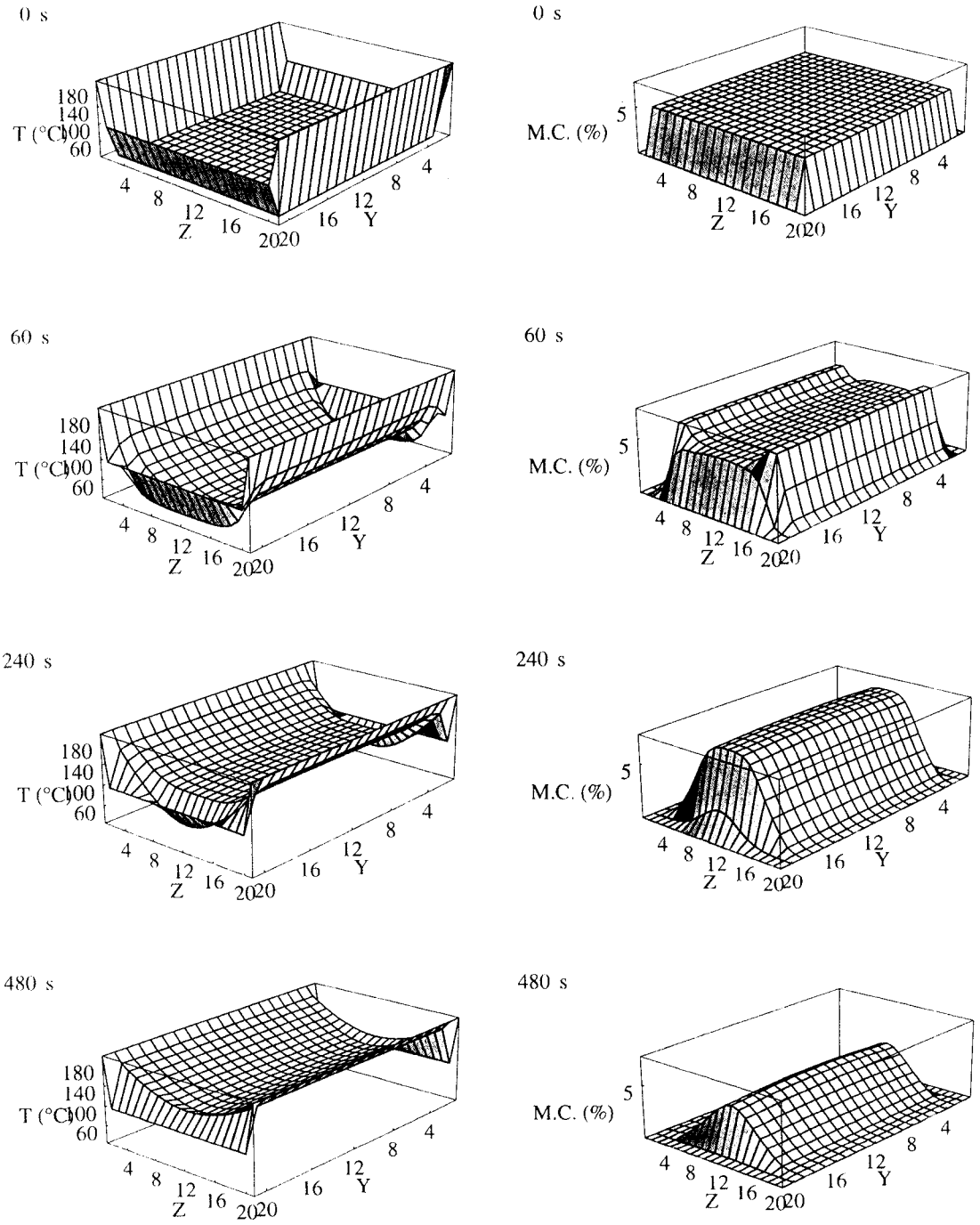

FIG. 3. Predicted temperature and moisture profiles during the hot-compression of a single-layer strandboard. The moisture content is the sum of the vapor and bound water content within the mat. The Y and Z coordinates designate the width and the thickness of the mat respectively. The boundary conditions are also depicted in the profiles. (Same interpretation of Y and Z, and the boundary conditions are also shown from Fig. 3 to Fig. 5.)

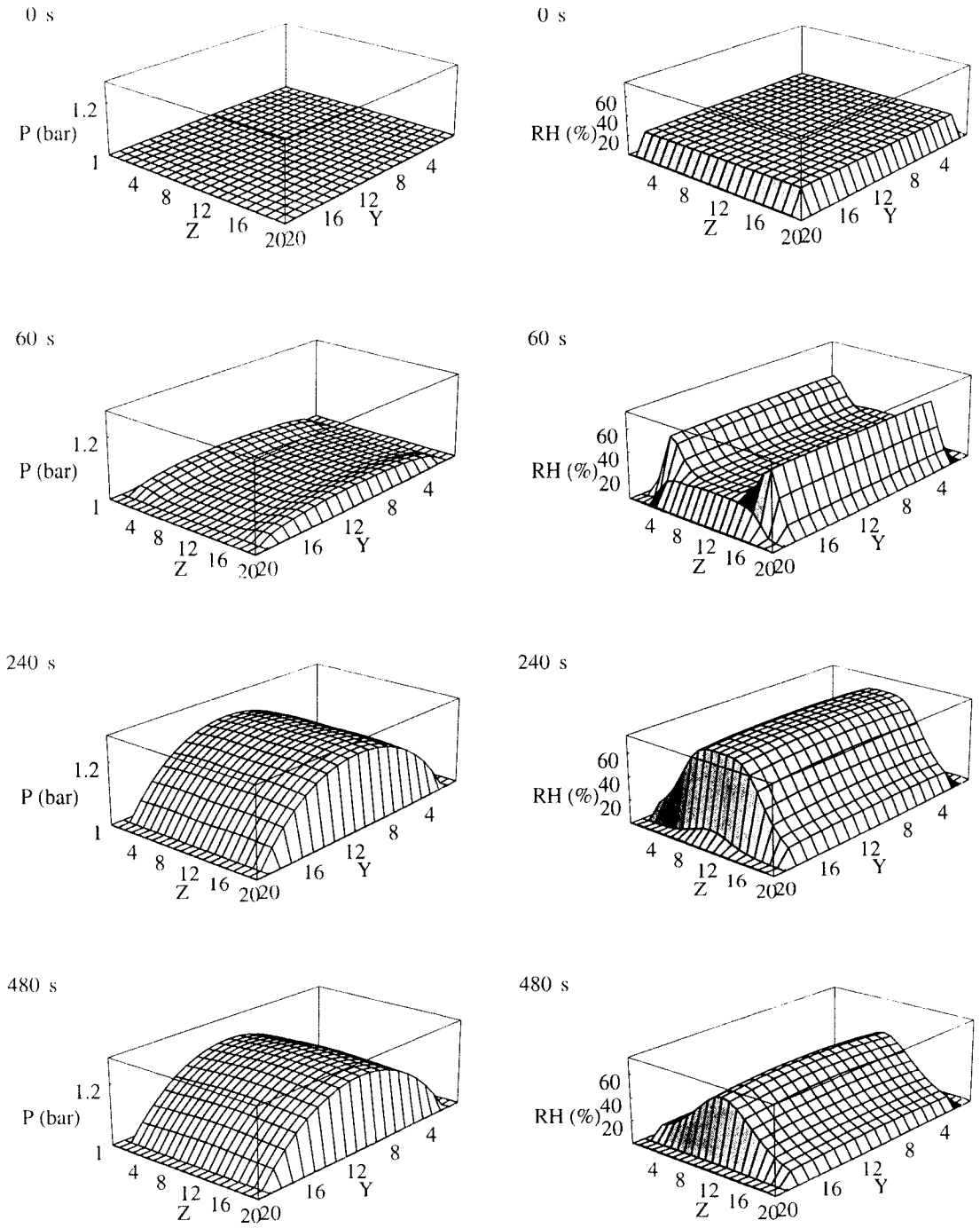

FIG. 4. Predicted total pressure and relative humidity (P, RH) profiles during the hot-compression of a single-layer strandboard. Total pressure is the sum of the partial air (p_a) and vapor (p_v) pressures. The relative humidity is calculated from the vapor pressure and the saturated vapor pressure at the given temperature.

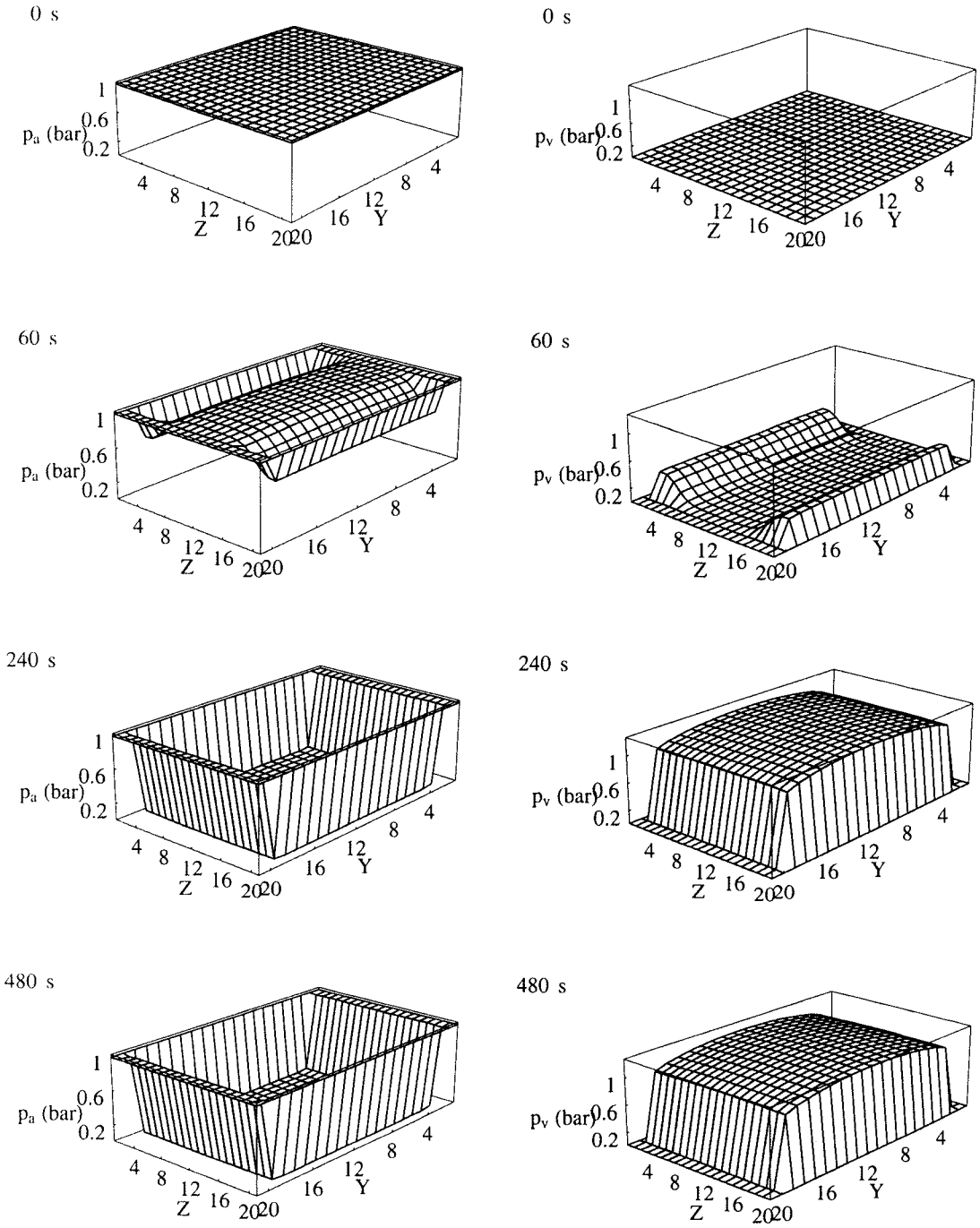

FIG. 5. Predicted partial air and vapor pressure (p_a, p_v) profiles during the hot-compression of a single layer strandboard.

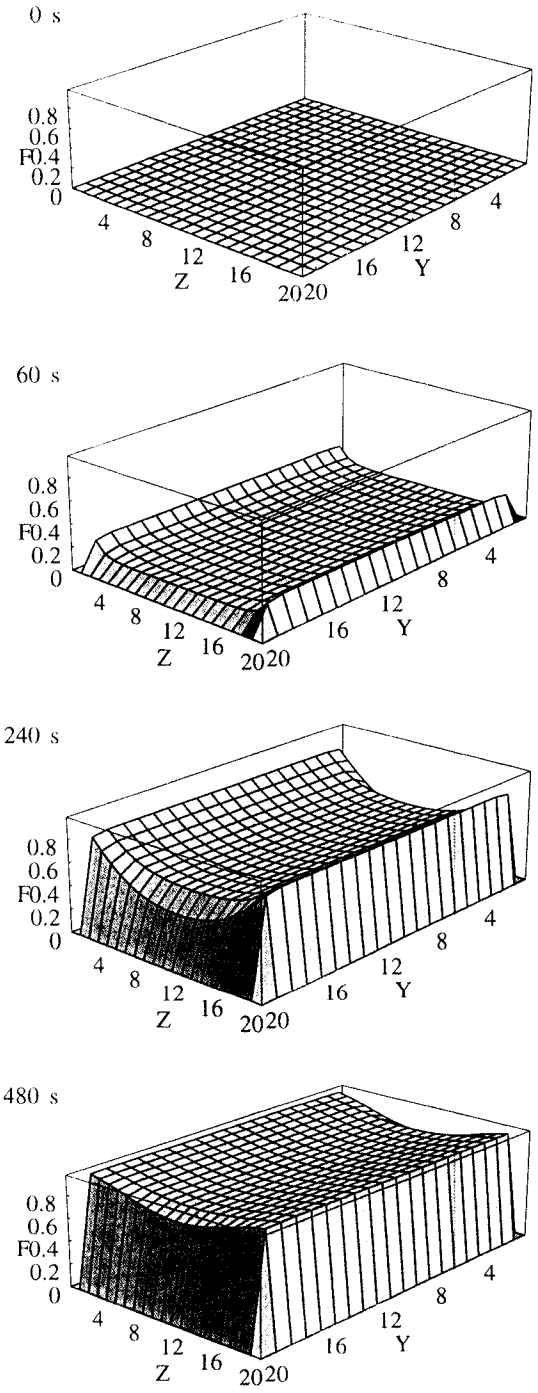

FIG. 6. Predicted adhesive cure index (F) profiles during the hot-compression of a single-layer strandboard. Cure index 1 designates the complete cure of the adhesive.

ture and vapor partial pressure gradient. The initial stage of the hot-compression is characterized by very intense vertical movement of heat and moisture.

Typical internal environment conditions are depicted in the middle of the press schedule (240 s). The surface temperature of the mat is getting closer to the hot platen temperature, and the center temperature gradually reaches the boiling point of water at the prevailing total pressure (Fig. 3). This triggers an intensive vaporization in the center location of the board. The partial pressure profiles (Fig. 5) confirm this phenomenon, where the vapor partial pressure increases sharply in the center location creating large pressure differentials between the center and the edges of the panel. The air partial pressure is low, implying that the majority of the air fraction of the gas phase is depleted. The total pressure increases far above the atmospheric pressure in the center of the panel (Fig. 4). The high total and partial vapor pressure differential drives the moisture horizontally towards the edges of the board, effectively reducing the moisture content (Fig. 3). The adhesive cure reaction is initiated through the whole cross section of the board, and is quite advanced at the surfaces (Fig. 6). The middle stage of the hot-compression is characterized by moderate vertical movement of heat and moisture and steady horizontal migration of moisture.

The last 240 seconds of the pressing cycle is less dynamic. At 480 seconds the end of the pressing period is reached and the venting begins in the hot-compression schedule. The surface of the board almost reaches the platen temperature. The heat slowly migrates towards the center of the mat, mainly by conduction. The initially vigorous flow of hot vapor ceases in the vertical direction, because there is no gradient in pressure (Fig. 4). The vaporization of the remaining water in the center is still active, which creates high relative humidity at this location (Fig. 4). The vapor generation can not keep up with the vapor losses at the edges, and both the partial vapor pressure and the total pressure drop in the center, diminish-

ing the initially large pressure differential in the horizontal direction. Therefore, the migration of vapor towards the edges gradually slows down, together with the moisture escape from the board. Note that, although the moisture is completely depleted at the surface of the board, there is still a considerable amount of water remaining in the center location (Fig. 3). Only a far longer simulated pressing period (~750 s) would be able to completely consume this moisture, and eliminate the pressure in the center of the board. However, at the end of a typical pressing schedule simulation the final total pressure in the center is around 1.3 bar, which if equilibrated too quickly, can result in a panel blow. An adequate venting period is crucial to eliminate the delamination of the panel. The polymerization reaction of the adhesive is still not complete (Fig. 6). The last stage of the hot-compression is characterized by very slow vertical movement of heat and moisture and diminishing horizontal migration of moisture. The three-dimensional profiles are powerful graphical tools to provide a better understanding of the relative magnitude and interaction of the different physical processes during the hot-compression.

SUMMARY AND CONCLUSIONS

The comprehensive experimental characterization of the heat and mass transfer process during hot-pressing is a formidable task due to the large number of interacting variables. A realistic mathematical model of the phenomena can make the task manageable. A one-dimensional drying model of hygroscopic porous materials was extended to two dimensions and adapted to include all the relevant heat and mass transfer mechanisms to simulate the hot-compression of wood-based composite panels. The model is capable of simulating the change of the internal environment within the vertical midplane of the flake mat in order to characterize the rapid moisture, temperature, and pressure gradient development, and the extent of the adhesive polymerization reaction in two dimensions.

The model was also extended to include the third spatial dimension, but the execution time became prohibitively long. Actually, the information gained by the three-dimensional model was irrelevant, when symmetric boundary conditions were assumed. The model is robust enough to simulate industrial pressing situations, including the press closing time and asymmetric boundary conditions. Events happening in the vertical direction are directly applicable to industrial board production, because they are not sensitive to the lateral size of the panel. However, predictions in the horizontal direction, especially at the edges, are dependent on the lateral dimension. Assigning different transport properties at different mesh points, the simulation of the hot-compression of a multilayer board is also attainable. In recent years nontraditional production technologies, such as high frequency heating, steam injection, or continuous pressing, are gaining acceptance in wood composite production. The model, with certain modifications, would be able to predict the internal environment of multilayer, full-size panels produced with one of these innovative technologies. The modular structure of the model computer code allows easy inclusion of research advancements, and therefore the process simulation can be further refined.

The hot-compression model allows one to carry out sensitivity analysis using the same mat structure. Process operators can gain insight into the effect of certain production parameters on the internal conditions of the mat, thus allowing them to make more informed decisions about the production process. Furthermore, by using this simulation model inside an optimization algorithm, the production parameters can be mathematically optimized to meet any specified objective.

ACKNOWLEDGMENTS

The financial contributions by the USDA National Research Initiative Competitive Grant Program, Grant 97-35504-4697, and the

Wood-Based Composite Center, Blacksburg, Virginia are greatly appreciated.

NOMENCLATURE

Constants

R = universal gas constant 8.31696 (J/mol/K)
M_a = molar weight of air 0.028968 (kg/mol)
M_v = molar weight of vapor 0.018016 (kg/mol)

Basic variables

Independent variables

t = time (s)
y = horizontal coordinate in the width of the board
z = vertical coordinate in the thickness of the board

Dependent variables

ρ_a = density of air (kg/m^3)
ρ_v = density of vapor (kg/m^3)
ρ_b = density of bound water (kg/m^3)
T = temperature (K)
F = extent of reaction (cure index)

Symbols

A = reaction constant
C = specific heat of wet wood (J/m^3/K)
C_p = heat capacity (J/kg/K)
D_{AB} = binary gas diffusivity for air–vapor mixture (m^2/s)
D_{eff} = effective gas diffusivity (m^2/s)
D_m = mat gas diffusivity (kg/m/s)
D_b = bound water diffusivity (kg s/m^3)
E = activation energy (J/mol)
G = heat generation (J/m^3)
K_g = specific gas permeability of dry wood (m^3/m)
K_m = mat superficial gas permeability (s)
L = board dimension (m)
P = total pressure (Pa)
S = entropy (J/mol/K)

c_p = heat convection flux (J/m^2/s)
h_p = enthalpy (J/kg)
k = thermal conductivity (J s/m/K)
n_p = mass flux (kg/m^2/s)
n = order of reaction
p_p = $\rho_p RT/\zeta_{vm} M_p$ partial pressure (Pa)
q = heat conduction flux (J/m^2/s)

α = attenuation factor for vapor diffusivity in the flakes
Θ = rotation angle (deg)
ϕ_1, ϕ_2 = degree of alignment (deg)
η = viscosity (kg/m/s)
λ = heat of vaporization (J/kg)
μ = chemical potential (J/kg)
ρ_d = density of dry wood (kg/m^3)
ζ_{lf} = lumen fraction in the flakes
ζ_{sm} = space fraction in the mat
ζ_{vm} = void (space + lumen) fraction in the mat
ζ_{lm} = lumen fraction in the mat

$\mathcal{H}^j$ = external heat transfer coefficient (J/m^2/s/K)
$\mathcal{K}^j$ = external bulk flow coefficient (m)
$\mathcal{D}^j$ = external diffusion coefficient (m/s)

Superscripts

B = boundary point
b = bottom boundary
j = represents boundaries (top, bottom, left, right)
l = left boundary
r = right boundary
t = top boundary
∞ = environment

Subscripts

L = longitudinal anatomical direction in solid wood
T = transverse (radial and tangential) anatomical direction in solid wood
a = air
b = bound water
cw = cell wall
d = dry wood
dp = dew point
f = flake
fsp = fiber saturation point
g = gas phase (air + vapor)
l = lumen (hole in the flake)
m = mat

p = phase (air, vapor, bound water)
s = space (hole in the mat)
sat = saturation
v = vapor
w = water

REFERENCES

AHMAD, M. 2000. Cure characteristics of phenol formaldehyde resin. Unpublished Report. Dept. of Wood Science and Forest Products, VPI & SU, Blacksburg, VA.

BEJAN, A. 1986. Convective heat transfer. John Wiley & Sons, New York, NY.

BOLTON, A. J., AND P. E. HUMPHREY. 1988. The hot-pressing of dry-formed wood-based composites. Part I. A review of the literature, identifying the primary physical process and the nature of their interaction. Holzforshung 42(6):403–406.

———, AND ———. 1994. The permeability of wood based composite materials. Holzforschung 48:95–100.

———, ———, AND P. K. KAVVOURAS. 1989a. The hot-pressing of dry formed wood-based composites. Part III. Predicted vapour pressure and temperature variation with time, compared with experimental data for laboratory boards. Holzforshung 43(4):265–274.

———, ———, AND ———. 1989b. The hot-pressing of dry formed wood-based composites. Part IV. Predicted variation of mattress moisture content with time. Holzforshung 43(5):345–349.

———, ———, AND ———. 1989c. The hot-pressing of dry formed wood-based composites. Part VI. The importance of stresses in the pressed mattress and their relevance to the minimization of pressing time, and the variability of board properties. Holzforshung 43(6): 406–410.

BOWEN, M. E. 1970. Heat transfer in particleboard during hot pressing. Ph.D. dissertation, Colorado State University, Fort Collins, CO.

CARVALHO, L. M. H., AND C. A. V. COSTA. 1998. Modeling and simulation of the hot-pressing process in the production of medium density fiberboard (MDF). Chem. Eng. Comm. 1701-21.

D'ONOFRIO, M. 1994. The superficial gas permeability of northeastern conifers and aspen flake composites. M.S. thesis, University of Maine, Orono, ME.

DAI, C., C. YU, AND P. HUBERT. 2000. Modeling vertical density profile in wood composites during hot-pressing. Proc. 5th Annual Pacific Rim Bio-Based Composites Symposium, Canberra, Australia.

HAILWOOD, A. J., AND S. HORROBIN. 1946. Absorption of water by polymers: Analysis in terms of a simple model. Trans. Faraday Soc. 42B:84–92.

HARLESS, T. E. G., F. G. WAGNER, P. H. SHORT, R. D. SEALE, P. H. MITCHELL, AND D. S. LADD. 1987. A model to predict the density profile of particleboard. Wood Fiber Sci. 19(1):81–92.

HATA, T. 1993. Heat flow in particle mat and properties of particleboard under steam-injection pressing. Wood Research, Bull. Wood Research Inst., Kyoto University 80:1–47.

———, S. KAWAI, R. EBIHARA, AND H. SASAKI. 1993. Production of particleboard with steam injection. Part V. Effect of particle geometry on temperature behaviors in particle mats and air permeabilities of boards. Mokuzai Gakkaishi 39(2):161–168.

HOLOPAINEN, T., L. ALVILA, J. RAINIO, AND T. T. PAKKAEN. 1997. Phenol-formaldehyde resol resin studied by C-NMR spectroscopy, gel permeation chromatography, and differential scanning calorimetry. J. Appl. Polymer Sci. 66:1183–1193.

HUMPHREY, P. E. 1989. The hot-pressing of dry-formed wood-based composites. Part II. A simulation model for heat and moisture transfer, and typical results. Holzforshung 43(3):199–206.

———, AND H. THOEMEN. 2000. The continuous pressing of wood-based panels: An analytical simulation model, its validation and use. Proc. 5th Annual Pacific Rim Bio-Based Composites Symposium, Canberra, Australia.

INCROPERA, F. P., AND D. P. DEWITT. 1996. Fundamentals of heat and mass transfer. John Wiley & Sons, New York, NY. 886 pp.

KAMKE, F. A., AND L. J. CASEY. 1988a. Gas pressure and temperature in the mat during flakeboard manufacture. Forest Prod. J. 38(3):41–43.

———, AND ———. 1988b. Fundamentals of flakeboard manufacture: Internal mat conditions. Forest Prod. J. 38(6):38–44.

KAUMANN, W. G. 1956. Equilibrium moisture content relations and drying control in superheated steam drying. Forest Prod. J. 25:328–332.

KAYIHAN, F., AND A. JOHNSON. 1983. Heat and moisture movement in wood composite materials during the pressing operation—A simplified model. Pages 511–531 *in* R. W. Lewis, K. Morgan, and B. A. Schrefler, eds. Numerical methods in heat transfer. Vol. II. John Wiley & Sons, Ltd.

KELLEY, M. W. 1977. Critical literature review of relationships between processing parameters and physical properties of particleboard. General Technical Report FPL-10, USDA Forest Serv., Forest Prod. Lab.

KIRAN, E., AND R. IYER. 1994. Cure behavior of paper-phenolic composite systems: Kinetic modeling. J. Appl. Polymer Sci. 51:353–364.

LENTH, C. A., AND F. A. KAMKE. 2001. Equilibrium moisture content of wood in high-temperature pressurized environments. Wood Fiber Sci. 33(1):104–118.

MAKU, T., R. HAMADA, AND H. SASAKI. 1959. Studies on the particleboard. Report 4: Temperature and moisture distribution in particleboard during hot-pressing. Wood Research Kyoto University pp. 934–946.

MYERS, G. E., A. W. CHRISTIANSEN, R. L. GEIMER, AND R. A. FOLLENSBEE. 1991. Phenol-formaldehyde resin cur-

ing and bonding in steam-injection pressing. I. Resin synthesis, characterization, and cure behavior. J. Appl. Polymer Sci. 43:237–250.

PATANKAR, S. V. 1980. Numerical heat transfer and fluid flow. McGraw-Hill Book Company, New York, NY. 197 pp.

PETZOLD, L. R., AND U. M. ASCHER. 1998. Computer methods for ordinary differential equations and differential-algebraic equations. SIAM, Philadelphia, PA. 314 pp.

SCHAJER, G. S., M. A. STANISH, AND F. KAYIHAN. 1984. A computationally efficient fundamental approach to drying of hygroscopic and non-hygroscopic porous materials. Proc. ASME Annual Meeting, New Orleans, LA.

SCOTT, E. P. 1989. Estimation of the thermal and kinetic properties associated with carbon/epoxy composite materials during curing. Ph.D. dissertation, Michigan State University, E. Lansing, MI.

SERNEK, M., F. A. KAMKE, AND I. M. SERNEK. 2000. Influence of temperature and time on the curing of UF adhesive. Wood Adhesive 2000 Extended Abstracts, Forest Products Society, Madison, WI.

SIAU, J. F. 1984. Transport processes in wood. Springer-Verlag, New York, NY.

———. 1995. Wood: Influence of moisture on physical properties. Department of Wood Science and Forest Products, V.P.I. & S. U., Blacksburg, VA. 227 pp.

SIMPSON, W. T. 1971. Equilibrium moisture content prediction for wood. Forest Prod. J. 21(5):48–49.

———. 1973. Predicting equilibrium moisture content of wood by mathematical models. Wood Fiber 5(1):41–49.

———. 1980. Sorption theories applied to wood. Wood Fiber 12(3):183–195.

———, AND H. N. ROSEN. 1981. Equilibrium moisture content of wood at high temperatures. Wood Fiber 13(3):150–158.

SKAAR, C. 1972. Water in wood. Syracuse University Press, Syracuse, NY.

SMITH, D. C. 1982. Wafer board press closing strategies. Forest Prod. J. 32(3):40–45.

STANISH, M. A., G. S. SCHAJER, AND F. KAYIHAN. 1986. A mathematical model of drying for hygroscopic porous media. AIChE Journal 32(8):1301–1311.

STRICKLER, M. D. 1959. Effects of press cycle and moisture content on properties of Douglas-fir flakeboard. Forest Prod. J. 9(7):203–215.

WOLFRAM, S. 1992. *Mathematica,* A System for doing Mathematics by Computer. Addison-Wesley Publishing Company, Reading, MA. 961 pp.

ZOMBORI, G. B., F. A. KAMKE, AND L. T. WATSON. 2001. Simulation of the mat formation process. Wood Fiber Sci. 33(4):564–579.